Nonequilibrium Molecular Dynamics Simulations of Diffusion of Binary Mixtures Containing Short *n*-Alkanes in Faujasite

Shaji Chempath,[†] Rajamani Krishna,[‡] and Randall Q. Snurr*,[†]

Department of Chemical and Biological Engineering and Center for Catalysis and Surface Science, Northwestern University, Evanston, Illinois 60208, and Department of Chemical Engineering, University of Amsterdam, Nieuwe Achtergracht 166, 1018 WV Amsterdam, The Netherlands

Received: March 14, 2004; In Final Form: June 16, 2004

We have used nonequilibrium molecular dynamics (NEMD) simulations to evaluate diffusivities for binary mixtures of methane/CF_4, propane/CF_4, *n*-butane/CF_4, and *n*-butane/ethane in zeolite faujasite at 300 K. A formula to estimate the error bars in the transport coefficients from NEMD is also presented. NEMD simulations can give cross coefficients of the Onsager matrix with considerably smaller error bars than those obtained from equilibrium MD (EMD). We evaluated diffusion coefficients that could not be evaluated previously using EMD. An estimation scheme based on the Maxwell−Stefan formulation was tested for predicting multicomponent diffusivities based on single component diffusion data. This estimation scheme works very well for the systems tested.

1. Introduction

Zeolites are microporous crystalline materials with intracrystalline channels of width 3−12 Å. They are widely used in the chemical industry for catalysis and separation applications. The diffusivity of physisorbed molecules in the channels of zeolites is an important parameter required for the design and optimization of these applications. Experimental studies and molecular modeling can be used to estimate the intracrystalline diffusivities. However, for many cases of diffusion in zeolites, the diffusivities obtained with different experimental techniques do not agree with one another. Molecular modeling can give insights into the microscopic mechanism of diffusion and may explain some of the discrepancies observed. In this paper we will discuss the use of a nonequilibrium molecular dynamics (NEMD) technique for calculating binary transport diffusivities in the zeolite faujasite. The results will also be used to test an estimation scheme based on the Maxwell−Stefan formulation, in which binary diffusivities are obtained from single-component data.

Many authors[1−7] have calculated the self-diffusivities of guest molecules in zeolite channels using molecular simulations, including both single components and mixtures. However, the Fickian diffusivity (also referred to as the transport diffusivity) is required in practical applications to describe diffusion in the presence of a concentration gradient. Some studies in the literature have reported the transport diffusivity of Lennard-Jones spheres in zeolites.[8−13] There have, however, been only a few studies[10,12,14,15] in the literature where multicomponent transport diffusivities from molecular simulations were reported. Industrial applications of zeolites or other microporous materials always involve multicomponent mixtures of molecules with more complicated shapes than simple spheres, and in this work we investigate multicomponent diffusion of small *n*-alkanes in the channels of faujasite. Faujasite is a large-pore zeolite composed of supercages of approximately 12 Å in diameter, tetrahedrally connected by 12-membered-ring windows of 7.5-Å diameter.[5] We study diffusion of four mixtures: methane/CF_4, propane/CF_4, butane/CF_4, and butane/ethane.

There are three main MD methods that are used to calculate transport diffusivities: dual control volume grand canonical molecular dynamics (DCV-GCMD), equilibrium molecular dynamics (EMD), and nonequilibrium molecular dynamics (NEMD). The DCV-GCMD method developed by Heffelfinger and Van Swol[16] involves the use of two control volumes located at the ends of a diffusion zone and maintained at different chemical potentials through insertion and deletion of particles. Ahunbay et al.[13] used this technique to study diffusion of methane through single-crystal silicalite membranes. Arya et al.[9] have shown that DCV-GCMD may give incorrect results if the ratio of insertions and deletions to molecular dynamics steps is not large enough. The second method, EMD, involves the use of Green−Kubo relations[17] to calculate the transport coefficients. This method has been used to calculate single and multicomponent diffusivities in zeolites.[10−12] Sanborn and Snurr[14] have shown that EMD might not work well for multicomponent systems at low loadings or when one species is very dilute. The third method uses an MD simulation with an extra external force (equivalent to a chemical potential gradient) applied on the molecules in the simulation to calculate the transport coefficients.[18] This method will be referred to as NEMD here. It has been used by Maginn and co-workers to calculate single-component diffusivities in microporous materials.[8,9] In this paper we will demonstrate that NEMD is more efficient than EMD for mixtures.

Since simulations and experiments for multicomponent diffusion are harder than single-component studies, it would be very useful to have theoretical methods for estimating multicomponent diffusivities from single-component data. Some such methods have been proposed in the literature[10,19,20] These methods, in general, involve the representation of the single-component diffusion data by using some parameters and then

* Author to whom correspondence should be addressed. Fax: 1-847-467-1018. Phone: 1-847-467-2977. E-mail: snurr@northwestern.edu.
[†] Northwestern University.
[‡] University of Amsterdam.

10.1021/jp048863s CCC: $27.50
Published on Web 08/06/2004

the estimation of mixture diffusivities from these parameters by a suitable model. However, it should be noted that single-component diffusion behavior itself can become quite complex depending on the sorbate molecule and the shape and connectivity of the zeolite channels. Molecular simulations can be used to test the validity of the binary diffusion estimation methods and the approximations involved. Skoulidas et al.[10] calculated both self-diffusivities and transport diffusivities of CH_4 and CF_4 in silicalite and then used a refinement and extension of the methodology suggested by Krishna and Baur[21] for estimation of binary diffusivities from single-component values. The binary diffusivities thus obtained were compared against those obtained directly from EMD mixture simulations and the agreement was found to be good. In this paper the validity of this scheme is tested for larger molecules with intramolecular degrees of freedom in the zeolite faujasite.

2. Theoretical Framework

2.1. Self-Diffusion and Transport Diffusion. The self-diffusivity (D_s) of a tagged particle diffusing through the intracrystalline space can be calculated with the Einstein expression,

$$D_s = \lim_{t\to\infty} \frac{\langle |r(t) - r(0)|^2 \rangle}{6t} \tag{1}$$

or using the velocity autocorrelation formalism

$$D_s = \frac{1}{3}\int_0^\infty \langle v(0)\cdot v(t)\rangle \, dt \tag{2}$$

Here r is the position vector and v is the velocity vector of the tagged particle.

The diffusion of a species under the influence of a concentration gradient is often called transport diffusion.[5] Fick's law of diffusion defines the transport diffusivity D_t as the proportionality factor between the flux J and the concentration gradient

$$J = -D_t \nabla c \tag{3}$$

In general D_t is not equal to the self-diffusivity.

2.2. Different Formulations of Transport Diffusion. Here we briefly review three different formulations for multicomponent diffusion in porous materials. All of them are equivalent, and given the parameters in one formulation we can always calculate the parameters in the other two formulations. It is important to specify the frame of reference with which we define the diffusion coefficients. In some cases the fluxes are calculated with respect to the center of mass of the system. Kamala et al.[15,22] used such a frame of reference for studying binary diffusion in slit pores and zeolite NaY. In the case of zeolite diffusion studied here, we assume that the zeolite crystal remains fixed and all fluxes are defined relative to this fixed frame of reference.

The Fickian equations for a mixture of two compounds in a zeolite are

$$J_1 = -D_{11}\nabla c_1 - D_{12}\nabla c_2 \tag{4}$$

$$J_2 = -D_{21}\nabla c_1 - D_{22}\nabla c_2 \tag{5}$$

On the basis of simulations of CH_4 and CF_4 in faujasite, Sanborn and Snurr[12] showed that the cross terms cannot always be neglected for diffusion of mixtures in zeolite membranes. For a multicomponent system the Fickian transport equations can be written in a matrix form

$$\mathbf{J} = -[\mathbf{D}]\nabla \mathbf{c} \tag{6}$$

where $\mathbf{J}$ and $\mathbf{c}$ are column vectors and $[\mathbf{D}]$ is the $N \times N$ diffusivity matrix.

The second formulation is based on nonequilibrium thermodynamics and considers chemical potential gradients as the fundamental driving forces for diffusion. This formulation is more convenient from a statistical mechanics or molecular simulations point of view. For binary diffusion in porous materials the transport equations are

$$J_1 = -L_{11}\nabla\mu_1 - L_{12}\nabla\mu_2 \tag{7}$$

$$J_2 = -L_{21}\nabla\mu_1 - L_{22}\nabla\mu_2 \tag{8}$$

where μ_i stands for the chemical potential of species i (units of kJ/mol). The L coefficients are sometimes referred to as Onsager coefficients. Onsager postulated that the $[\mathbf{L}]$ matrix is symmetric.[23] $[\mathbf{D}]$ can be calculated as

$$[\mathbf{D}] = [\mathbf{L}][\mathbf{\Gamma}] \tag{9}$$

where the elements of the square matrix $[\mathbf{\Gamma}]$ are given by

$$\Gamma_{ij} = \frac{RT}{c_j}\frac{d\ln f_i}{d\ln c_j} \tag{10}$$

f is the fugacity, and c_j is the concentration of species j inside the zeolite.

A detailed introduction to the Maxwell−Stefan (MS) formulation and a description of the physical significance of various parameters can be found in the review article by Krishna and Wesselingh.[24] The Maxwell−Stefan (MS) diffusivities for diffusion in porous materials are defined as follows

$$-\nabla\mu_i = RT\sum_{j=1,j\neq i}^{n}\frac{\theta_j(u_i - u_j)}{Đ_{ij}} + RT\frac{u_i}{Đ_i} \tag{11}$$

where u_i is the velocity of species i with respect to the zeolite and θ_j is the fractional occupancy of the species j. Fractional occupancy is the ratio of loading (n_i, molecules/supercage) to the saturation loading ($n_{i,s}$, molecules/supercage).

$$\theta_i = \frac{n_i}{n_{i,s}} \tag{12}$$

The MS diffusivities $Đ_i$ may be interpreted as inverse friction coefficients describing the mobility of species i in the zeolite. The exchange coefficients $Đ_{ij}$ reflect the correlation effects in binary mixture diffusion as discussed by Skoulidas et al.[10]

2.3. Onsager Formulation for Tracer Diffusion. In this section we will briefly discuss the Onsager formulation for diffusion of tagged particles. Consider the diffusion of a *single* species through the zeolite pores. Let the number of particles be N. We will tag some of the particles as 1 and the rest 2. N_1 and N_2 are the number of particles of type 1 and 2, respectively, and $N = N_1 + N_2$. The Green−Kubo relations[6,17] for the Onsager coefficients in the binary diffusion case can be written as

$$L_{11} = \frac{1}{3Vk_BT}\int\langle\sum_{l=1}^{N_1} v_{1,l}(0)\cdot\sum_{m=1}^{N_1} v_{1,m}(t)\rangle \, dt \tag{13}$$

$$L_{12} = \frac{1}{3Vk_BT}\int\langle\sum_{l=1}^{N_1} v_{1,l}(0)\cdot\sum_{m=1}^{N_2} v_{2,m}(t)\rangle \, dt \tag{14}$$

The correlation function can be split into self-functions and cross functions as done by Theodorou and Maginn[6,8] previously

$$L_{11}^{\text{self}} = \frac{1}{3Vk_BT}\int\langle\sum_{l=1}^{N_1} v_{1,l}(0)\cdot v_{1,l}(t)\rangle\, dt \quad (15)$$

$$L_{11}^{\text{cross}} = \frac{1}{3Vk_BT}\int\langle\sum_{l=1}^{N_1}\sum_{m=1,m\neq l}^{N_1} v_{1,l}(0)\cdot v_{1,m}(t)\rangle\, dt \quad (16)$$

where $L_{11} = L_{11}^{\text{self}} + L_{11}^{\text{cross}}$. The equation for the self-term can be simplified in terms of a one-particle correlation function, and the equation for the cross term can be simplified in terms of correlations between two different particles:

$$L_{11}^{\text{self}} = ac_1 \quad (17)$$

where

$$a = \frac{1}{3k_BT}\int\langle v_{1,l}(0)\cdot v_{1,l}(t)\rangle\, dt \quad (18)$$

Here $c_1 = N_1/V$ is the concentration of particles of type 1. Also $c_1 = \rho_z n_{1,s}\theta_1$, where ρ_z is the density of zeolite (unit cells/m^3). Note that $a = D_s/k_BT$. Similarly

$$L_{11}^{\text{cross}} = bc_1^{\,2} \quad (19)$$

where

$$b = \frac{V}{3k_BT}\int\langle v_{1,l}(0)\cdot v_{1,m}(t)\rangle\, dt \quad (20)$$

where the angular brackets indicate an ensemble average and $v_{1,l}$ is the velocity of the lth particle of type 1. Note that all the equations in this section up to this point are valid for multicomponent diffusion as well as tagged particle diffusion. The remaining equations in this section (eqs 21−26) are only for tagged particle diffusion in a single component system. Then

$$L_{11} = ac_1 + bc_1^{\,2} = \alpha\theta_1 + \beta\theta_1^{\,2} \quad (21)$$

$$L_{12} = bc_1c_2 = \beta\theta_1\theta_2 \quad (22)$$

$$L_{22} = ac_2 + bc_2^{\,2} = \alpha\theta_2 + \beta\theta_2^{\,2} \quad (23)$$

$$L_{21} = bc_2c_1 = \beta\theta_2\theta_1 \quad (24)$$

where $\alpha = \rho_z n_s a$ and $\beta = (\rho_z n_s)^2 b$.

An equation for L_{11} in terms of the Đ coefficients can be written and compared to eq 21. In case of tracer diffusion this leads to

$$\frac{\alpha}{\beta} = \frac{1/Đ_1}{1/Đ_{11}} \quad (25)$$

For tracer diffusion $Đ_{12} = Đ_{21} = Đ_{11}$.

$$\frac{\alpha}{\beta} = \frac{a}{b\rho_z n_s} = \frac{\int\langle v_{1,l}(0)\cdot v_{1,l}(t)\rangle\, dt}{\rho_z n_s V\int\langle v_{1,l}(0)\cdot v_{1,m}(t)\rangle\, dt} \quad (26)$$

In general we would expect the above quantity to decrease with loading because self-correlation will decrease with loading and cross correlation will increase with loading. This expectation will be tested below. Equations 25 and 26 connect important parameters required in the MS formulation to correlations from statistical mechanics.

TABLE 1: Force-Field Parameters for Zeolite−Sorbate and Sorbate−Sorbate Interactions[a]

nonbonded	ϵ/k_B, K	σ, Å
CH_4-CH_4	147.95	3.73
CH_3-CH_3	72.0	3.923
CH_2-CH_2	72.0	3.923
CF_4-CF_4	134.0	4.662
CH_4-O	133.3	3.214
CH_3-O	83.8	3.364
CH_2-O	83.8	3.364
CF_4-O	109.57	3.734

bond angle	k_θ, kJ rad^{-2}	θ_0, deg
C−C−C	259.8	114

torsion	a_0/k_B, K	a_1/k_B, K	a_2/k_B, K	a_3/k_B, K
C−C−C−C	0.0	355.0	−68.2	791.3

[a] Lennard-Jones parameters for other sorbate−sorbate interactions were obtained with the combining rules of $\epsilon_{ij} = \sqrt{\epsilon_i\epsilon_j}$ and $\sigma_{ij} = (\sigma_i + \sigma_j)/2$. A harmonic potential was used for the bond angle bending ($\mathcal{T}(\theta) = k_\theta(\theta - \theta_0)^2$). Torsion angle potentials were treated with the cosine-expansion form $\mathcal{T}(\phi) = a_0 + a_1(1 + \cos(\phi)) + a_2(1 - \cos(2\phi)) + a_3(1 + \cos(3\phi))$.

3. Transport Coefficients from Molecular Dynamics Simulation

NEMD or EMD can be used to evaluate the members of the [**L**] matrix. The Green−Kubo relations[6,17] which involve the evaluation of correlations between species velocities as shown in eqs 13 and 14 can be used to evaluate L_{ij} from EMD. In NEMD a mechanical force F_j is applied on each molecule of species j in the MD simulation and the average flux $\langle J_i\rangle$ of species i is measured from the simulation. Then L_{ij} are evaluated as

$$L_{ij} = \frac{\langle J_i\rangle}{F_j} \quad (27)$$

By applying a mechanical force on species j, we are adding an extra potential to the energy of the system. This is equivalent to applying a chemical potential gradient to the system. In our MD simulation code all molecules are assigned a property called "color charge".[8,25] All molecules of species j are given a color charge of 1. All molecules of other species are assigned a color charge of 0. During the MD run only the molecules with nonzero color charge feel the external force. In the case of multiatomic molecules, the color charge on each atom is proportional to its mass and the sum of color charge on a molecule is equal to 1. This is equivalent to applying the force F_j on the center of mass of the multiatomic molecule. The term color charge is used to make it clear that this is not an electrostatic charge in the force field.

3.1. Force Field. We have performed EMD and NEMD calculations for single-component diffusion of methane, ethane, propane, butane, and CF_4 in zeolite faujasite for various fractional loadings. For consistency with previous simulations from our research group,[12,14,26] we considered a completely siliceous form of faujasite without cations. Mixture simulations were performed for mixtures of methane/CF_4, propane/CF_4, butane/CF_4, and ethane/butane. Force field parameters for intermolecular interactions are listed in Table 1. They are the

same as those used by Sanborn and Snurr.[12,14] The intramolecular parameters for bond-bending and torsion potentials were taken from the literature[27,28] and can be found in Table 1. Alkane bond lengths were kept fixed. Atomic coordinates of the faujasite atoms were taken from the neutron diffraction work of Hriljac et al.[29] The interaction of silicon atoms with the guest molecules was neglected in the force field, as is common. The zeolite framework was considered rigid and a pretabulated potential map was used for the Lennard-Jones interactions between zeolite oxygen atoms and adsorbed Lennard-Jones centers.[30] Sorbate molecules were modeled using the united atom model for methylene and methyl groups. Methane and CF_4 were also modeled as united atoms. All intermolecular interactions were truncated at 12.1 Å. Typically each simulation contained 64−100 mobile sorbate molecules. The unit cell of faujasite contains 8 supercages. Depending on the loading, we used 2 to 8 unit cells with periodic boundary conditions.

3.2. Thermostats. Different types of thermostats[31] are available in the literature for keeping the temperature of a system constant during an MD simulation. Two of them were implemented in our simulation code[32] and tested for use during an NEMD simulation. Note that the external force does work on the system during an NEMD simulation, and the heat generated should be removed to keep the system at constant temperature. Different thermostats accomplish this task by using different mechanisms. It is necessary to verify that no artificial effects are introduced by the thermostat. Our results below indicate that all thermostats tested show the same behavior. We have implemented two slightly different versions of the Nose−Hoover thermostat and will refer to them as NH1 and NH2. The NH1 thermostat acts on all particles of the system and maintains the overall temperature of the system. The NH2 thermostat acts separately on each species and controls the temperature of each species independently. Another thermostat referred to as a Gaussian thermostat keeps the kinetic temperature $T_{K,i}$ of each species in the system constant. Kinetic temperature of species i, $T_{K,i}$, is defined so that

$$\frac{N_i d_i k_B T_{K,i}}{2} = E_{K,i} \tag{28}$$

where d_i is the number of degrees of freedom for one molecule, $E_{K,i}$ is the total kinetic energy of species i, and N_i is the number of molecules of species i. Note that kinetic energy has to be defined with respect to a reference frame. Two types of Gaussian thermostats (referred to as Gauss1 and Gauss2) were used here. In Gauss1 the zeolite frame of reference is chosen, which implies that the thermostat is acting on all degrees of freedom ($N_i d_i$ of them). In Gauss2 kinetic energy is defined by removing the degrees of freedom corresponding to the center of mass of the diffusing species. Here there are only $N_i d_i - 3$ degrees of freedom. However, it should be noted that all other quantities (velocities, fluxes) reported in this paper are defined with respect to the absolute frame of reference, where the zeolite is kept fixed. All four thermostats (NH1, NH2, Gauss1, and Gauss2) were tested as shown in section 4.1.

Two finite-difference integration schemes were tested for integrating the equations of motion. A 6th order Gear predictor−corrector integration scheme (Gear6)[31] was implemented in combination with the NH1 and NH2 thermostats. A leapfrog integration scheme as given by Brown and Clarke[33] was implemented for use with Gauss1 and Gauss2. After testing the different integration schemes and thermostats as described below, we decided to use Gear6 and NH2 for all the remaining simulations.

3.3. EMD Implementation. In EMD a regular NVT-MD simulation is done and species velocities are written to a file every 0.1 ps. For a run of 10 ns this leads to storing of 100 000 velocity values in a disk file. The average velocity (the velocity of center of mass) of each species in the system is calculated separately and written to the disk file. The simulations were run for an equilibration period of 1 ns and a production run of 10 ns. Flux correlation functions (eqs 13 and 14) between different species were calculated from the stored velocities. These correlation functions were integrated with respect to time numerically by using Simpson's rule. We have tested the numerical integration with different intervals between writing the velocities to the disk file. In our simulations, the numerical integration error coming from the use of a 0.1-ps interval is rather small. So an interval of 0.1 ps was used in all EMD simulations. A smaller write interval (say 0.02 ps) can be used for more accurate integrations, but this will lead to storing of many more configurations in the disk file. Data from the same EMD simulations were also used to calculate the self-diffusivities. The self-diffusivities were calculated with use of Einstein's formula (eq 1), and this required storing the position of each particle every 1 ps in a disk file. Both Nose−Hoover (NH1 and NH2) and Gaussian thermostats (Gauss1 and Gauss2) were tested to check the effect of different thermostats on EMD. All of them gave the same results for a CH_4/CF_4 system at a total loading of 1 molecule/unit cell and 50% methane. In all other EMD simulations we have used the NH2 thermostat with the Gear6 algorithm.

3.4. NEMD Implementation. For binary diffusion in zeolites, there are four transport coefficients to be evaluated: L_{11}, L_{12}, L_{21}, and L_{22}. An NEMD simulation with force applied on species 1 can be used to calculate two of them: L_{11} and L_{21}. During such a simulation the fluxes of species 1 and 2 are calculated separately and eq 27 is used to evaluate the L coefficients. Similarly a simulation with force applied on species 2 can be used to evaluate L_{12} and L_{22}. Onsager's reciprocity theorem states that $L_{12} = L_{21}$. This equality can be used as a check on the simulations.

In all simulations the external force was applied in the x-direction and the flux in the x-direction was measured. The evaluation of flux J_i during the simulation was done as follows:

$$\langle J_i \rangle = \rho_i \langle v \rangle = \rho_i \frac{1}{\tau_s} \int_0^{t=\tau_s} \left(\frac{1}{N_i} \sum_k v_{i,k} \right) \mathrm{d}t \tag{29}$$

where ρ_i is the particle density (in molecules/Å^3) and τ_s is the time span of the simulation (in ps). Note that the average velocity $\langle v \rangle$ is calculated over all the particles of species i and also over the length of the simulation. By taking the integral inside the summation and substituting $\rho_i = N_i/V$,

$$\langle J_i \rangle = \frac{1}{V\tau_s} \sum_k \int_0^{t=\tau_s} v_{i,k} \, \mathrm{d}t \tag{30}$$

$$\langle J_i \rangle = \frac{1}{V\tau_s} \sum_k [r_{ik}(\tau_s) - r_{ik}(0)] \tag{31}$$

Thus, only the final positions and initial positions of all particles are needed for evaluation of the average flux.

3.5. Calculation of Thermodynamic Factors. The evaluation of Γ_{ij}, the thermodynamic factors mentioned in eq 9, was done with use of data obtained from binary grand canonical Monte Carlo (GCMC) simulations. Adsorption isotherms were generated for adsorption from a gas of fixed mole fraction and

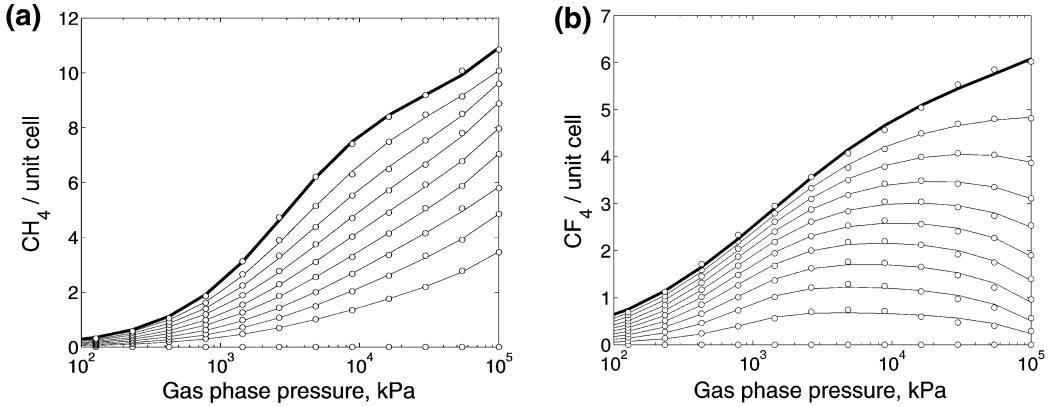

Figure 1. Mixture adsorption isotherms of CH_4 and CF_4 in faujasite at 300 K. Each curve corresponds to a particular gas-phase composition y_{CH_4}. In the figure on the left, the $y_{CH_4} = 0$ curve lies on the x axis;, the $y_{CH_4} = 1.0$ curve is the topmost curve shown as a thick black line. $y_{CH_4} = 0.1$, 0.2,0.3, 0.4, 0.5, 0.6, 0.7, 0.8, and 0.9 lie in between. In the figure on the right the $y_{CH_4} = 0$ curve is the topmost and the $y_{CH_4} = 1.0$ curve lies on the x axis. For each case the symbols represent the data from GCMC and the lines represent eq 32.

temperature but varying pressure. The loading of each species was obtained as a function of total pressure in the gas phase and these data were fitted to a semiempirical isotherm equation[34] of the form

$$n(P) = KP\left[1 + \left(\frac{KP}{a(1+\kappa P)}\right)^c\right]^{(-1/c)} \qquad (32)$$

where n is the loading of the species in molecules/supercage, P is the gas-phase pressure, K is the Henry's law constant, a is a measure of saturation loading, κ represents an adsorbed phase compressibility, and c determines the curvature of the isotherm. From each binary GCMC run we obtained two isotherms (one for each compound) and thus two sets of fitting parameters. This process was repeated for different values of y_i, the mole fraction of species i in the gas phase. Assume that isotherms have been evaluated at $y_{i,1}, y_{i,2}, ..., y_{i,k}$. Each of the $2k$ isotherms was fitted to eq 32 to obtain $2k$ different sets of parameters. The values of isotherm parameters corresponding to any y_i that lie between $y_{i,l}$ and $y_{i,l+1}$ were estimated by linearly interpolating with respect to y_i. The evaluation of Γ_{ij} for given loading (n_i, n_j) was done numerically as follows.

$$\Gamma_{ij} = \frac{RT}{\rho_z}\frac{\ln[f_i(n_i, n_j + dn)] - \ln[f_i(n_i, n_j)]}{dn} \qquad (33)$$

This involved the evaluation of fugacities f_i at two loadings: (n_i, n_j) and (n_i, $n_j + dn$). The values of P and y_i that minimize the error from the specified loading (n_i, n_j) were found by a random search. Then the fugacity was evaluated as $f_i = Py_i$. Similarly the fugacity corresponding to (n_i, $n_j + dn$) also was evaluated and then eq 33 was used to evaluate Γ_{ij}. The isotherms for CH_4/CF_4 adsorption in faujasite at 300 K are given in Figure 1. The empirical equation fits quite well with the simulations results. For CH_4/CF_4 and other mixtures the isotherm-equation parameters are reported as a function of gas-phase composition y elsewhere.[35]

4. Results

4.1. Comparison of Simulation Algorithms. To test the new NEMD code, we calculated the L coefficients for binary diffusion of CH_4/CF_4 mixtures and compared them against the values obtained by Sanborn and Snurr[12] using EMD. All the main-term coefficients (L_{11} and L_{22}) were found to be within 10% and all the cross coefficients (L_{21} and L_{12})were found to be within 20%. Tests were done at two different loadings (2 and 4 molecules/supercage) and different mole fractions (0.25, 0.50, and 0.75). In addition, we ran all the single component simulations below using both EMD and NEMD. In most cases the single component L coefficients obtained with the two methods agreed with each other within an accuracy of 4%. The maximum deviation observed was 10%.

To check the effect of different thermostats, a set of simulations were done for an equimolar mixture of CH_4 and CF_4 in faujasite at 300 K with the four different thermostats mentioned above. Total loading was 2 molecules/supercage. These simulations were repeated at different values of the applied force, too (0.04−0.67 kJ/(mol Å)). The flux obtained from the simulations is plotted as a function of the force in Figure 2. The curves indicate that the response of the system is linear up to an applied force of 0.33 kJ/(mol Å). Left panel of Figure 2 shows that different thermostats start to behave differently at high values of applied force. This is because the applied force does work on the system and leads to heating of the system. These four thermostats remove the heat from the system in different ways, and this leads to different results at such high applied force. The rest of the simulations reported here were done with applied forces in the range 0.12−0.33 kJ/(mol Å) and using the Gear6 integration scheme and the NH2 thermostat.

4.2. Single Component Diffusion. Single-component diffusion of methane, ethane, propane, butane, and CF_4 in faujasite was investigated with both EMD and NEMD. Self-diffusivities (D_s) and Onsager coefficients (L) were evaluated from EMD simulations. L coefficients were also evaluated from the NEMD simulations. The results from EMD had an estimated error of 10%, whereas the estimated error for L from NEMD was only 2%. See Appendix A for error estimation formulas. Figure 3 shows the results from MD simulations of methane at 300 K at various loadings. A scheme based on the Maxwell−Stefan (MS) formulation of diffusion where single component diffusion data are used to predict mixture diffusion is explained in Appendix B. We will refer to this scheme as the "MS estimation scheme". Continuous lines show the fit to the MS estimation scheme as described by eqs 41−44 in the appendix. Figure 3 shows that the transport diffusivity D_t reaches a maximum around a fractional loading of 0.6. This is a result of increases in both L and the thermodynamic factor Γ. Another way of looking at this is as follows: D_t can be written as the product of Đ and d ln f/d ln c. The term d ln f/d ln c increases monotonically, following $1/(1-\theta)$, for single-site Langmuir isotherm behavior. For multisite adsorption the isotherm exhibits inflection behav-

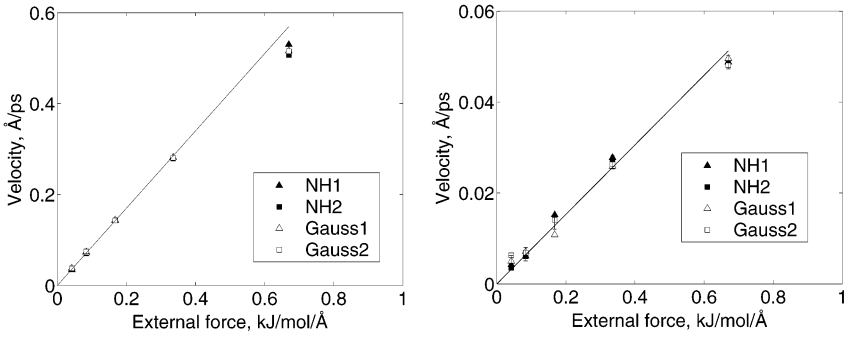

Figure 2. Average velocity of methane (left) and CF_4 (right) in the direction of the applied force from NEMD simulations of an equimolar methane/CF_4 mixture in faujasite. Four sets of data are shown corresponding to four different thermostats. An external force is applied on methane. Simulations were done at 300 K and a total loading of 2 molecules/supercage. The line represents a linear fit passing through the origin.

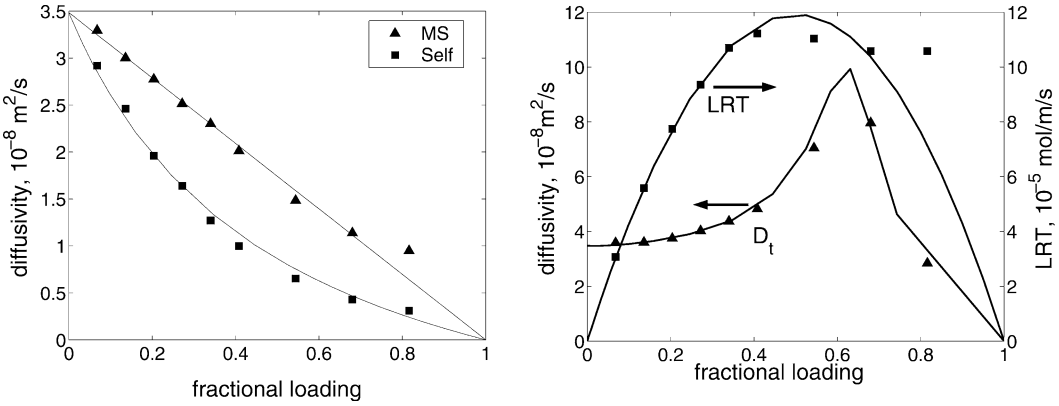

Figure 3. D_s (self), Đ (Maxwell−Stefan $Đ_1$), D_t (transport), and L (Onsager) for CH_4 in faujasite at 300 K. On the left, the lines represent predictions according to eqs 41−44. On the right, the lines represent D_t and L calculated from Đ. D_t is plotted on the left y axis and *LRT* is plotted on the right y axis. The symbols represent values obtained from single component MD simulations.

ior. This is the case for CH_4 in faujasite. As a consequence of the inflection, that occurs at a loading of 10 molecules per cage, the thermodynamic correction factor exhibits a sharp maximum at this loading. The factor d ln f/d ln c decreases when the loading increases beyond 10 molecules per cage and then increases again as saturation loading is approached. The value of *LRT* obtained from simulations does not agree well with the MS estimation scheme at high loadings (last data point on the right panel of Figure 3). This is because the assumption that Đ varies linearly with loading is not true at higher loadings for this system. We will, however, use the linear approximation for MS estimations to keep the number of parameters to a minimum (see Appendix B).

Results for other molecules are given in Figure 4. In all cases of single-component diffusion, the MS diffusivity seems to be a linear function of the fractional loading as suggested by eq 43. Equations 41 and 43 can be used to represent the single-component diffusion data with just two parameters for each species, $Đ_i(0)$ and ζ_i, as described in the appendix. Similar calculations were performed by Skoulidas and Sholl for diffusion of various Lennard-Jones spheres in silicalite.[36] It was found that the variation of Đ as a function of fractional loading roughly falls into two categories. In some cases it decreases as a linear function of the fractional loading. This is similar to the behavior of a lattice gas and was referred to as the "strong confinement" scenario.[10] In other cases Đ was found to remain a constant and these were referred to as the "weak confinement" scenario. In a more recent paper[11] they investigated the effect of different pore shapes. For some combination of pore shapes and sorbates Đ initially increased with loading. In our current study in faujasite we see that Đ decreases linearly with loading similar to the strong confinement scenario. Using lattice models, Bhide and Yashonath[37,38] studied the different factors that affect diffusivity vs concentration trends. However, currently there is no way of quantitatively predicting these trends a priori other than MD simulation. The mechanism of single-component diffusion in zeolite pores is still not well understood. There are many factors that may affect the observed diffusion behavior. The strength of the interaction between the probe molecule and the pore wall, and the size of the probe will affect the diffusion behavior. The velocity correlations between neighboring particles are also important. The adsorption pattern also is important. At low loading the molecules tend to adsorb at the lowest energy sites, but at higher loading they may rearrange to adsorb in some other pattern. Since all the above factors are important in deciding the Đ vs loading trend, it might not always be possible to classify the single-component diffusion behavior as "strong" or "weak" confinement.

4.3. Binary Diffusion. The L coefficients for binary mixture diffusion of CH_4/CF_4 in faujasite are reported in Figure 5. NEMD was able to give converged results with error bars of less than 10% for most of the cross coefficients. For the runs with a low loading of 1 molecule/supercage the error bars in L_{12} and L_{21} were about 20%. However, EMD did not converge for these conditions even after a 40-ns run. Thus NEMD appears to be very efficient in calculating the L coefficients accurately. Sanborn and Snurr[14] were also not able to calculate the L coefficients at a low loading of 1 molecule/supercage with EMD. Figure 5 shows that at a given number of molecules/supercage the L_{11} coefficient increases with the mole fraction of species 1. Similarly L_{22} increases with the mole fraction of species 2. The cross coefficients vary roughly as an inverted parabola as the mole fractions vary from zero to one. The results of the MS estimation (described in Appendix B) are shown as lines

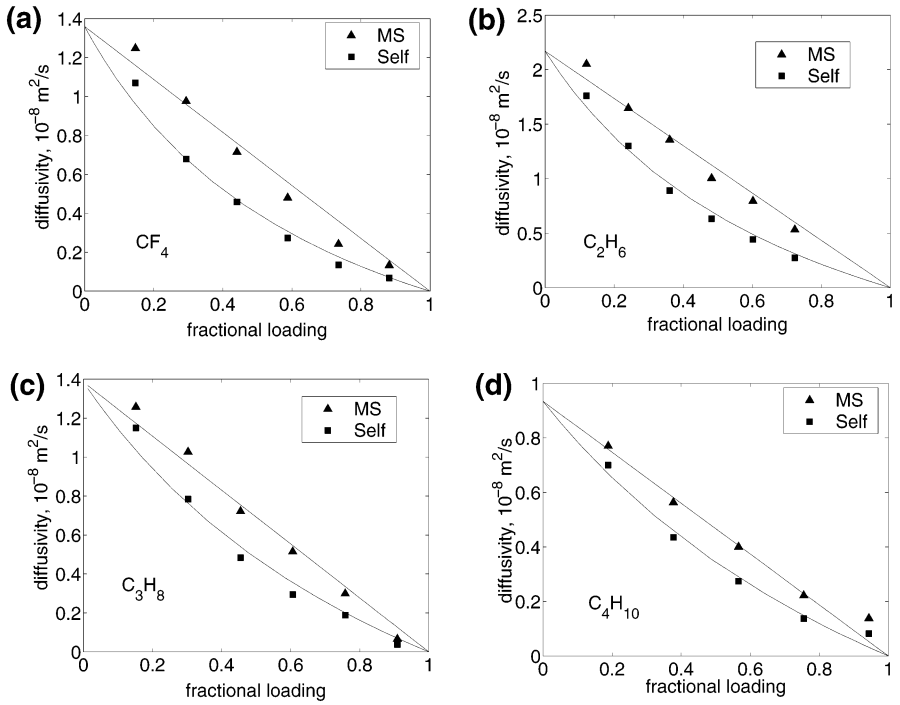

Figure 4. Pure component Đ and D_s for CF_4 (a), C_2H_6 (b), C_3H_8 (c), and C_4H_{10} (d) in faujasite at 300 K. The lines represent predictions according to eqs 41 and 43.

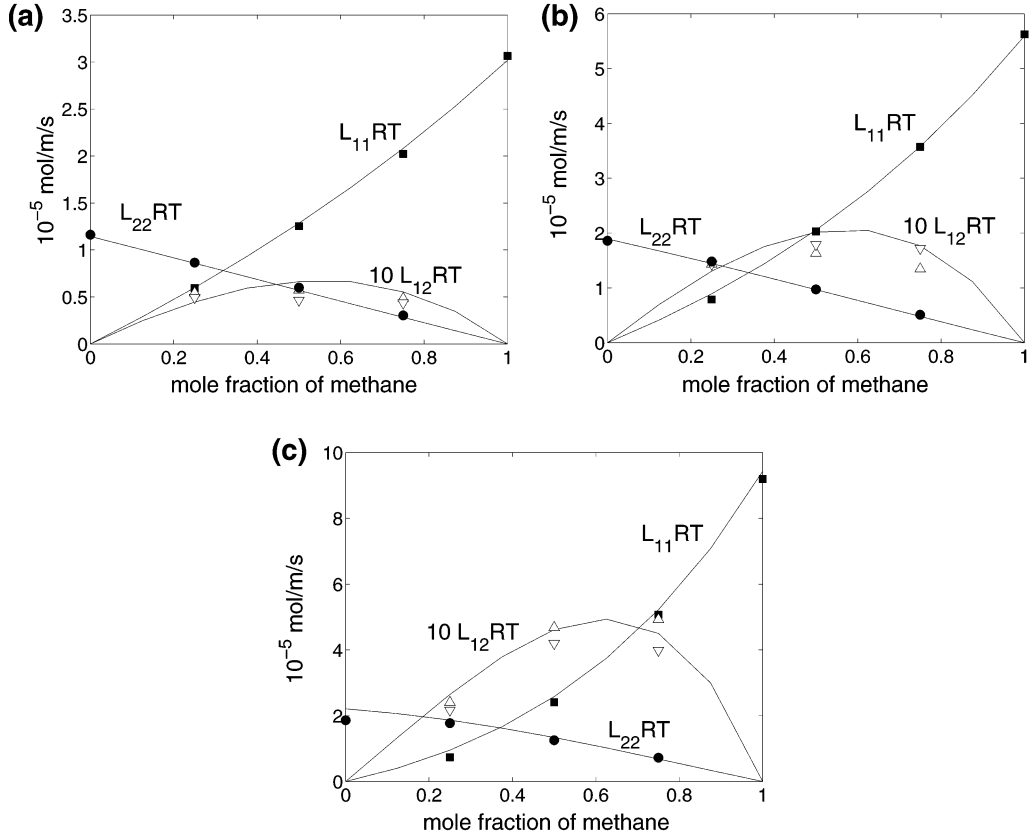

Figure 5. L_{ij} coefficients from NEMD simulations of methane (1) and CF_4 (2) in faujasite at 300 K. The lines represent predictions according to MS estimations. The squares, up triangles, down triangles, and circles represent L_{11}, L_{12}, L_{21}, and L_{22}, respectively. The cross coefficients (L_{12} and L_{21}) are scaled by a factor of 10, so that they can be plotted on the same y axis. Total loading: (a) 1 molecule/supercage, (b) 2 molecules/supercage, and (c) 4 molecules/supercage.

in Figure 5. The lines agree remarkably well with the symbols which represent the binary simulation data.

Results for C_3H_8/CF_4, C_4H_{10}/CF_4, and C_4H_{10}/C_2H_6 are shown in Figure 6. This is the first time that binary transport diffusivities of nonspherical molecules such as butane and propane in faujasite are being reported from MD simulations. The estimated error in cross coefficients is less than 10%. Again, the predictions from the MS estimation agree quite well with the binary simulation results. The results here indicate that the approximations involved in the MS estimation scheme hold very

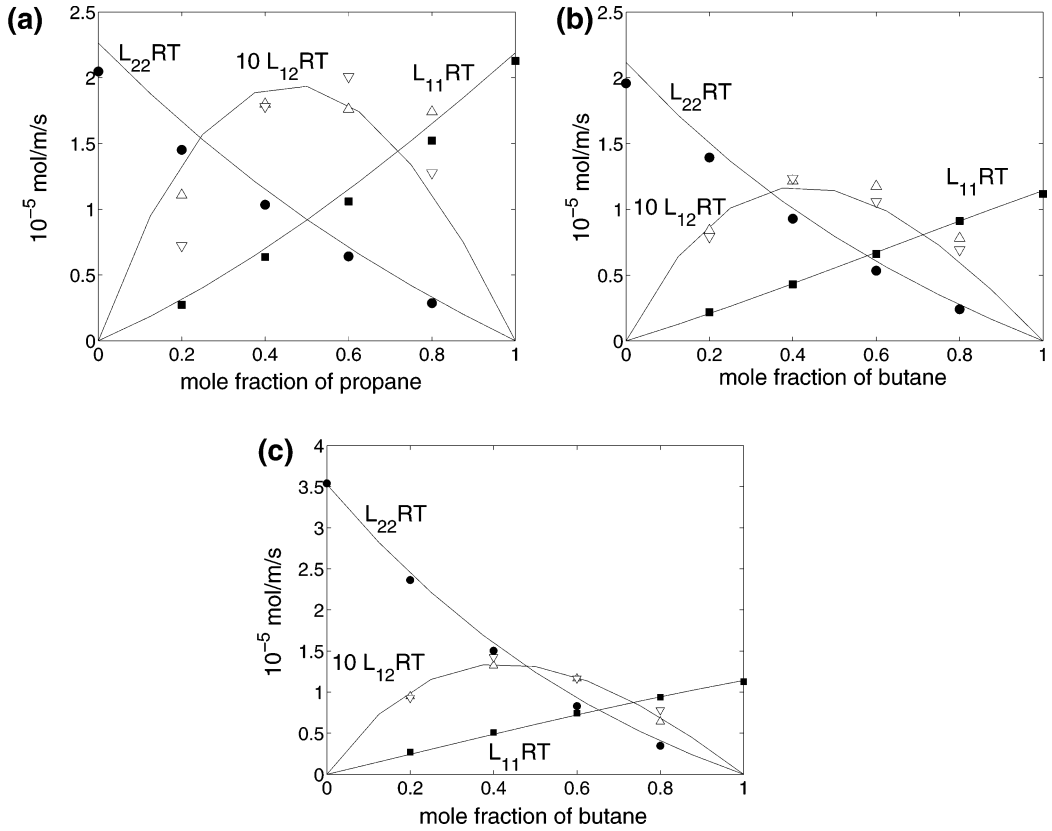

Figure 6. L_{ij} coefficients from NEMD simulations: (a) propane (1) and CF_4 (2) in faujasite at 300 K for a total loading of 3.125 molecules/supercage; (b) butane (1) and CF_4 (2) in faujasite at 300 K for a total loading of 2.5 molecules/supercage; and (c) butane (1) and ethane (2) in faujasite at 300 K for a total loading of 2.5 molecules/supercage. The lines represent predictions according to MS estimations. The squares, up triangles, down triangles, and circles represent L_{11}, L_{12}, L_{21}, and L_{22}, respectively. The cross coefficients (L_{12} and L_{21}) are scaled by a factor of 10, so that they can be plotted on the same y axis.

well even in the case of nonspherical molecules such as butane and propane. The estimations here were based on four parameters obtained from the data for single components. These four parameters are $Đ_1(0)$, $Đ_2(0)$, ζ_1, and ζ_2 (see Appendix B). These parameters were evaluated from a series of single-component calculations of self-diffusivity and transport diffusivity. They can be used to predict diffusivities in various mixtures over the whole range of compositions. We can also use the MS formulation as a parameter-fitting scheme. Thus any binary mixture diffusion data at a given temperature and varying composition can be represented in terms of four parameters.

An important assumption in the MS estimation scheme is that $Đ_1(\theta_1,\theta_2)$ is a function of total loading $\theta = \theta_1 + \theta_2$ only. In Figure 7 we plot $Đ_i$ values of each compound, obtained from our binary simulations, against the total loading. The values are normalized by dividing by $Đ_i(0)$, the pure component Maxwell diffusivity at zero loading (see Table 2). It is clear that the $Đ$ values obtained from multicomponent simulations show the same behavior as the single-component $Đ$ values (see Figures 3 and 4).

In the MS estimation scheme (Appendix B) we studied the variation of single-component diffusion (both D_s and $Đ$) as a function of fractional loading and then parametrized the data in terms of $Đ_1$ and $Đ_{11}$. It was assumed that these quantities have the same values in the multicomponent case as in the single-component case, at a given value of total fractional loading θ. Equivalently we may do the parametrization using the particle correlations α and β too. As in the case of MS estimation α and β may also be assumed to be functions of total loading only. The functional form in eqs 21−24 suggests that the L_{11} will increase with θ_1 and L_{12} will initially increase and then decrease (inverted parabola) for the cases of tracer diffusion. In our mixture results where we keep the total loading constant and vary the compositions also we see approximately similar trends. The main terms increase with loading and the cross terms plotted versus composition look roughly like an inverted parabola.

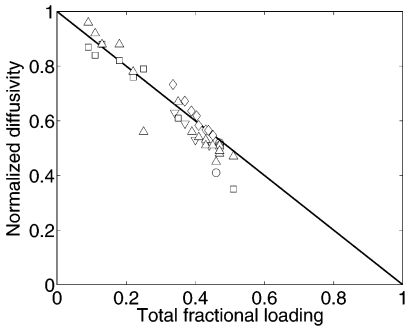

Figure 7. $Đ_i$values calculated from binary simulations are plotted as a function of total loading. The x axis is the total fractional loading θ (see eq 46). $Đ_i$ values are normalized by dividing by $Đ_i(0)$ taken from Table 2. The solid line represents the expected behavior from the MS estimation scheme. Data for methane (squares), ethane (down triangles), propane (circles), butane (diamonds), and CF_4 (up trangles) are shown. This plot is constructed from the information in Figures 5 and 6.

4.4. Comparison of Error from EMD and NEMD. In appendix A we have described different ways of calculating the error bars for the L coefficients obtained from EMD and NEMD. Equation 37 is very useful because it can be applied before running the simulation itself. For the case of CH_4/CF_4 the error in L_{12} predicted by using eq 37 and the observed errors are plotted in Figure 8. The error decreases with increasing

TABLE 2: Parameters that Describe Single Component Diffusion in Faujasite at 300 K[a]

molecule	$n_{i,sat}$	$Đ_i(0)$	ζ_i
CH_4	14.7	3.48	0.49
C_2H_6	8.3	2.17	0.78
C_3H_8	6.6	1.39	1.13
C_4H_{10}	5.3	0.93	1.40
CF_4	6.8	1.36	0.82

[a] $Đ_i(0)$ has the units of 10^{-8} m^2/s, and ζ_i is dimensionless. The saturation values reported here are the loadings at 300 K and 10^7 kPa in units of molecules/supercage.

simulation time. The results on the left of Figure 8 are from an NEMD run with applied force of 0.13 kJ/(mol Å) for a loading of 4 molecules/supercage and 50% CH_4 at 300 K. Observed errors are defined according to eq 38. Observed errors from an EMD run at the same condition are also reported in Figure 8 (see Appendix A). It can be seen that the predicted and observed errors from NEMD match well. Also, for a given simulation time, the errors observed from EMD are in general higher than those from NEMD.

Similar calculations were also done for CH_4/CF_4 at 1 molecule/supercage, 300 K, and 25% CH_4 with an applied force of 0.33 kJ/(mol Å). In this case the errors from EMD are far higher than those from NEMD, as shown on the right of Figure 8. EMD simulations require the evaluation of flux correlation functions in order to evaluate the L coefficients. The flux correlation functions between CH_4 and CF_4 at 1 molecule/supercage and 25% CH_4 are shown in Figure 9. We expect these correlation functions, $\langle v_1(0)v_2(t)\rangle$ and $\langle v_2(0)v_1(t)\rangle$, to be equal so that Onsager's reciprocal relations ($L_{12} = L_{21}$) are satisfied. From the difference between the two correlation functions it can be concluded that these flux correlation functions have not converged. This is the reason for the observed large EMD error in L_{12} in Figure 8.

At low loadings the cross coeffcients may become very small and negligible compared to the main coefficients. Equation 7 shows that the flux of species 1 depends on gradients of chemical potentials of both species. If $\nabla\mu_1$ is zero then the flux of species 1 depends entirely on the cross coefficient L_{12}. Even if L_{12} is small (less than one-tenth of L_{11}) it has to be evaluated accurately to evaluate the flux. Sanborn and Snurr[12] have previously demonstrated that there are situations where the cross coefficients cannot be neglected.

5. Conclusions

We have used NEMD to evaluate binary diffusivities of various mixtures in the zeolite faujasite at 300 K. A formula to estimate the error bars in the L coefficients is also presented. Using this formula the expected error bars can be calculated before starting the simulation. NEMD simulations can give cross coefficients of the L matrix with considerably smaller error bars than those obtained from EMD. The Onsager coefficients for diffusion of binary mixtures of small alkanes and CF_4 are calculated within acceptable error bars. These are results that could not be obtained previously with EMD.

We applied an estimation scheme based on the Maxwell−Stefan formulation of diffusion where multicomponent diffusivities were predicted based on single-component diffusion data. Four parameters obtained from single-component diffusivities of two compounds are used to predict binary diffusivities at any composition. This MS estimation scheme suggested by Krishna and co-workers appears to work very well to describe diffusion of binary mixtures containing short alkanes and CF_4 in faujasite.

Acknowledgment. This work has been supported by the U.S. National Science Foundation.

Appendix A. Estimation of Error During NEMD

In EMD and NEMD the L coefficients are calculated by using ensemble averages from the simulation. These ensemble averages will converge only if the simulations are done for a very long time. Depending on the length of the simulations there may be significant statistical errors in the estimated L coefficients. Sometimes the simulation is repeated with different starting conditions and the standard deviation is used as a measure of error. The alternate systematic way in which we have estimated the errors is presented below.

During an NEMD simulation, the flux is measured as given by eq 31, or equivalently:

$$\langle J_i\rangle = \rho\langle v_i\rangle = \frac{N_i}{V}\sum_k \frac{1}{N_i}\frac{[r_{ik}(\tau_s) - r_{ik}(0)]}{\tau_s} \tag{34}$$

The standard deviation in $\langle J\rangle$ can be evaluated as the standard deviation of the sum on the right-hand side of eq 34. Let the true value of average velocity $\langle v\rangle$ of species i due to the applied force be v_∞. This true value can be obtained only if we run the simulation for infinite time. Values obtained from a simulation of finite time τ_s with a finite number of particles N_i will have a value of $v_\infty \pm \delta v$. The expected value of $[r(\tau_s) - r(0)]$ for each particle after a simulation of time τ_s is $v_\infty\tau_s$. In addition to the overall movement in the direction of applied force, each molecule has a self-diffusion-like motion. This self-diffusion of each particle introduces a deviation of $\pm\sigma$ to the displacement of the particle. σ is the standard deviation in the displacement of the particle because of self-diffusion only. For the Brownian motion of a particle

$$\sigma = \sqrt{2D_{s,i}\tau_s} \tag{35}$$

The standard deviation for $\langle v\rangle$, which is calculated as the average over N_i particles, will be

$$\delta v = \frac{\sqrt{(2D_{s,i}\tau_s)}}{\tau_s}\frac{1}{\sqrt{N_i}} = \sqrt{\frac{2D_{s,i}}{N_i\tau_s}} \tag{36}$$

The standard deviation in the value of L_{ij} with force F_e applied on species j will be

$$\delta L_{ij} = \frac{\rho_i}{F_e}\sqrt{\frac{2D_{s,i}}{N_i\tau_s}} \tag{37}$$

If the order of magnitude of the self-diffusion coefficient of species i is known then the expected error from simulation can be evaluated by using the above formula.

We can also estimate the error in the flux J from a simulation by looking at the flux-components perpendicular to the applied field. When a force is applied in the x-direction there should not be a resultant flux in the y- or z-direction. However, there will be some small value of flux in any simulation because of the statistical error coming from the finite size of the simulation. The magnitude of this flux can be considered as another estimate

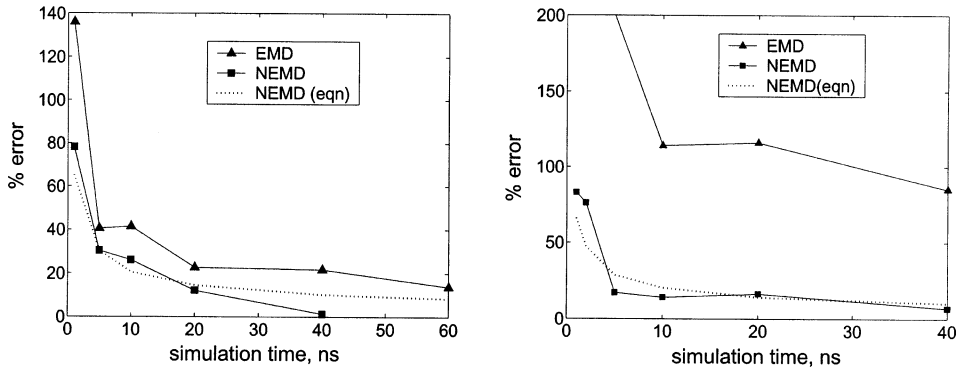

Figure 8. Percent error in L_{12} from NEMD and EMD for CH_4 and CF_4 in faujasite at 300 K for a total loading of (a) 4 molecules/supercage with 50% CH_4 and (b) 1 molecule/supercage with 25% CH_4. The filled symbols connected by solid lines are the error observed from simulations. The dashed line is the error estimated by using eq 37.

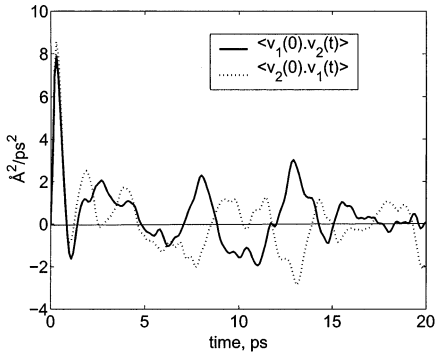

Figure 9. Flux correlation functions for calculating L_{12} and L_{21} from EMD. These are evaluated from a 40-ns run of a CH_4 (1)/CF_4 (2) mixture in faujasite at 300 K for a total loading of 1 molecule/supercage and 25% methane.

of error. During NEMD simulations fluxes in all 3 directions are evaluated and another error estimate is obtained as

$$\delta J_x = \frac{|J_y| + |J_z|}{2} \tag{38}$$

In EMD the L_{ij} are evaluated by eqs 13 and 14. On the right-hand side of the equation there is a dot product of two vector quantities. This can be expanded as the sum of three components

$$L_{ij} = \frac{\int_0^\infty \langle j_{i,x}(0)j_{j,x}(t) + j_{i,y}(0)j_{j,y}(t) + j_{i,z}(0)j_{j,z}(t)\rangle \, \mathrm{d}t}{3Vk_BT} \tag{39}$$

$$L_{ij} = (L_{ij}^{xx} + L_{ij}^{yy} + L_{ij}^{zz})/3 \tag{40}$$

For simulations with cubic symmetry all three L_{ij} on the right-hand side of eq 40 should be equal. The standard deviation between these 3 values can be used as an estimate of the error on L_{ij} obtained from an EMD simulation.

Appendix B. Estimation of Binary Diffusivities with MS Estimation Scheme

The MS estimation scheme described below is based on the works of Krishna and co-workers.[10,24] This scheme can be used to estimate binary MS diffusivities from information about self-diffusion and transport diffusion of single components.

On the basis of single-component tracer diffusion, an inverse friction coefficient $Đ_{11}$ for friction between particles of the same species can be defined as

$$\frac{1}{D_{s,1}} = \frac{1}{Đ_1} + \frac{\theta}{Đ_{11}} \tag{41}$$

where θ is the fractional coverage

$$\theta = n/n_{sat} \tag{42}$$

Here n and n_{sat} are the loading and saturation loading, respectively. $Đ_1$ is the MS diffusivity and $D_{s,1}$ is the self-diffusivity. These diffusivities can be evaluated from pure component MD simulations as a function of θ. Then $Đ_{11}$ can be evaluated by using eq 41. For all simulations in faujasite it was found that the single-component MS diffusivity varies linearly as suggested by

$$Đ_1(\theta) = Đ_1(0)[1 - \theta] \tag{43}$$

The ratio of $Đ_{11}$ to $Đ_1$ is found to be more or less a constant. We define

$$\zeta_1 = Đ_{11}/Đ_1 \tag{44}$$

Skoulidas et al.[10] fitted the value of ζ_1 to a weakly decreasing function of θ. From our simulations also we found the calculated values of ζ_1 to be slowly decreasing with θ. However, to keep the number of parameters to a minimum, ζ_1 is assumed to be a constant for each species.

Thus the single-component data of species i at a given temperature are parametrized by two constants $D_i(0)$ and ζ_i. Note that at very low loading $Đ_1(0) = D_{s,1}(0) = D_t(0)$. The parameters that describe the single-component diffusion of various molecules in faujasite at 300 K are given in Table 2.

For binary diffusion the fractional loadings are defined as follows

$$\theta_1 = n_1/n_{1,sat} \qquad \theta_2 = n_2/n_{2,sat} \tag{45}$$

$$\theta = \theta_1 + \theta_2 \tag{46}$$

To describe binary diffusion in the MS formulation by using eq 11, four values are required: $Đ_1$, $Đ_2$, $Đ_{12}$, and $Đ_{21}$. For binary diffusion in zeolites, the Onsager reciprocity relation leads to the constraint $n_{2,sat}Đ_{12} = n_{1,sat}Đ_{21}$ as derived by Skoulidas et al.[10] It is assumed that $Đ_1$ and $Đ_2$ are functions of the total

fractional coverage θ only. They are assumed to follow the same θ dependence as in the single-component case. Thus,

$$Đ_1(\theta_1,\theta_2) = Đ_1(0)[1-\theta] \tag{47}$$

$$Đ_2(\theta_1,\theta_2) = Đ_2(0)[1-\theta] \tag{48}$$

Another assumption is that $Đ_{12}$, the friction between species 1 and 2, lies between $Đ_{11}$ and $Đ_{22}$. A logarithmic interpolation[10] is used to estimate $Đ_{12}$:

$$n_{2,\mathrm{sat}}Đ_{12} = [n_{2,\mathrm{sat}}Đ_{11}]^{\theta_1/(\theta_1+\theta_2)}[n_{1,\mathrm{sat}}Đ_{22}]^{\theta_2/(\theta_1+\theta_2)} \tag{49}$$

By interchanging the subscripts 1 and 2 for all the terms above, $Đ_{21}$ can be obtained. The $Đ_{11}$ and $Đ_{22}$ at the given loading are obtained as

$$Đ_{11} = \zeta_1 Đ_1(\theta) \quad \text{and} \quad Đ_{22} = \zeta_2 Đ_2(\theta) \tag{50}$$

Thus, using eqs 44−50 and parameters $Đ_1(0)$, $Đ_2(0)$, ζ_1, and ζ_2 we can predict mixture diffusion at any composition.

Appendix C. Relation between *L* and MS Diffusivity

By using an MS estimation scheme the **L** matrix for a binary system can be calculated from single-component data. The equations used to relate the Onsager matrix **L** to the MS coefficients $Đ_1$, $Đ_2$, and $Đ_{12}$ are given below. They can be derived by equating the fluxes written in two formalisms (Onsager and Maxwell−Stefan). It can be shown that

$$L_{11} = \frac{\rho}{RT|B|}\left[\frac{1}{Đ_2} + \frac{\theta_1}{Đ_{21}}\right]\theta_1 n_{1,\mathrm{sat}} \tag{51}$$

$$L_{12} = \frac{\rho}{RT|B|}\left[\frac{\theta_1}{Đ_{12}}\right]\theta_2 n_{1,\mathrm{sat}} \tag{52}$$

$$L_{22} = \frac{\rho}{RT|B|}\left[\frac{1}{Đ_1} + \frac{\theta_2}{Đ_{12}}\right]\theta_2 n_{2,\mathrm{sat}} \tag{53}$$

$$L_{21} = \frac{\rho}{RT|B|}\left[\frac{\theta_2}{Đ_{21}}\right]\theta_1 n_{2,\mathrm{sat}} \tag{54}$$

where $|B|$ is the determinant of matrix [**B**] defined as:

$$B_{ii} = \frac{1}{Đ_i} + \sum_{k=1,k\neq i}^{2}\frac{\theta_k}{Đ_{ik}} \qquad B_{ij(i\neq j)} = -\frac{\theta_i}{Đ_{ij}} \tag{55}$$

References and Notes

(1) Auerbach, S. M. *Int. Rev. Phys. Chem.* **2000**, *19*, 155−198.
(2) Bates, S. P.; Van Santen, R. A. *Adv. Catal.* **1998**, *42*, 1−114.
(3) Demontis, P.; Suffritti, G. B. *Chem. Rev.* **1997**, *97*, 2845−2878.
(4) Keil, F. J.; Krishna, R.; Coppens, M. O. *Rev. Chem. Eng.* **2000**, *16*, 71−197.
(5) Kärger, J.; Ruthven, D. M. *Diffusion in Zeolites*; Wiley: New York, 1992.
(6) Theodorou, D. N.; Snurr, R. Q.; Bell, A. T. In *Comprehensive Supramolecular Chemistry*; Alberti, G., Bein, T., Eds.; Pergamon: Oxford, UK, 1996; Vol. 7, pp 507−548.
(7) Nagumo, R.; Tabaka, H.; Nakao, S. *J. Phys. Chem. B* **2003**, *107*, 14422−14428.
(8) Maginn, E. J.; Bell, A. T.; Theodorou, D. N. *J. Phys. Chem.* **1993**, *97*, 4173−4181.
(9) Arya, G.; Chang, H. C.; Maginn, E. J. *J. Chem. Phys.* **2001**, *115*, 8112−8124.
(10) Skoulidas, A. I.; Sholl, D. S.; Krishna, R. *Langmuir* **2003**, *19*, 7977−7988.
(11) Skoulidas, A. I.; Sholl, D. S. *J. Phys. Chem. A* **2003**, *107*, 10132−10141.
(12) Sanborn, M. J.; Snurr, R. Q. *AIChE J.* **2001**, *47*, 2032−2041.
(13) Ahunbay, M. G.; Elliott, J. R.; Talu, O. *J. Phys. Chem. B* **2002**, *106*, 5163−5168.
(14) Sanborn, M. J.; Snurr, R. Q. *Sep. Purif. Technol.* **2000**, *20*, 1−13.
(15) Kamala, C. R.; Ayappa, K. G.; Yashonath, S. *Phys. Rev. E* **2002**, *65*, 061202 (1−11).
(16) Heffelfinger, G. S.; Van Swol, F. *J. Chem. Phys.* **1994**, *100*, 7548−7552.
(17) Zhou, Y.; Miller, G. H. *J. Phys. Chem.* **1996**, *100*, 5516−5524.
(18) Evans, D. J.; Morriss, G. P. *Statistical Mechanics of Nonequilibrium Liquids*; Academic Press: London, UK, 1990.
(19) Krishna, R. *Chem. Phys. Lett.* **2000**, *326*, 477−484.
(20) Sundaram, N.; Yang, R. T. *Chem. Eng. Sci.* **2000**, *55*, 1747−1754.
(21) Krishna, R.; Baur, R. *Sep. Purif. Technol.* **2003**, *33*, 213−254.
(22) Kamala, C. R.; Ayappa, K. G.; Yashonath, S. *J. Phys. Chem. B* **2004**, *108*, 4411−4421.
(23) Yourgrau, W.; van der Merwe, A.; Raw, G. *Treatise on Irreversible and Statistical Thermophysics*; The Macmillan Company: New York, 1966.
(24) Krishna, R.; Wesselingh, J. A. *Chem. Eng. Sci.* **1997**, *52*, 861−911.
(25) Sarman, S.; Evans, D. J. *Phys. Rev. A* **1992**, *46*, 1960−1966.
(26) Clark, L. A.; Ye, G. T.; Gupta, A.; Hall, L.; Snurr, R. Q. *J. Chem. Phys.* **1999**, *111*, 1209−1222.
(27) Siepmann, J. I.; Martin, M. G.; Mundy, C. J.; Klein, M. L. *Mol. Phys.* **1997**, *90*, 687−693.
(28) Jorgensen, W. L.; Madura, J. D.; Swenson, C. J. *J. Am. Chem. Soc.* **1984**, *106*, 6638−6646.
(29) Hriljac, J. A.; Eddy, M. M.; Cheetham, A. K.; Donohue, J. A.; Ray, G. J. *J. Solid State Chem.* **1993**, *106*, 66−72.
(30) June, R. L.; Bell, A. T.; Theodorou, D. N. *J. Phys. Chem.* **1990**, *94*, 8232−8240.
(31) Allen, M. P.; Tildesley, D. J. *Computer Simulation of Liquids*; Oxford University Press: Oxford, UK, 1987.
(32) Gupta, A.; Chempath, S.; Sanborn, M. J.; Clark, L. A.; Snurr, R. Q. *Mol. Simul.* **2003**, *29*, 29−46.
(33) Brown, D.; Clarke, J. H. R. *Mol. Phys* **1984**, *51*, 1243−1252.
(34) Heuchel, M.; Snurr, R. Q.; Buss, E. *Langmuir* **1997**, *13*, 6795−6804.
(35) Chempath, S. Molecular Simulation of Multicomponent Adsorption and Diffusion in Zeolites, Ph.D. Thesis, Northwestern University, 2004.
(36) Skoulidas, A. I.; Sholl, D. S. *J. Phys. Chem. B* **2002**, *106*, 5058−5067.
(37) Bhide, S. Y.; Yashonath, S. *J. Chem. Phys* **1999**, *111*, 1658−1657.
(38) Bhide, S. Y.; Yashonath, S. *J. Phys. Chem. B* **2000**, *104*, 2607−2612.